

Joining of highly aluminum-doped lanthanum strontium manganese oxide with tetragonal zirconia by plastic deformation

John V. Spirig^{a,c}, Jules L. Routbort^b, Dileep Singh^{b,*}, Graham King^a,
Patrick M. Woodward^a, Prabir K. Dutta^{a,c,*}

^a Department of Chemistry, The Ohio State University, 100 West 18th Avenue, Columbus, Ohio 43210, United States

^b Argonne National Laboratory, 9700 South Cass Avenue, Argonne, IL 60439, United States

^c The Center for Industrial Sensors and Measurement, 177 Watts Hall, 2041 College Road, Columbus, OH 43210, United States

Received 30 September 2007; received in revised form 12 February 2008; accepted 24 March 2008

Abstract

Aluminum-doped lanthanum strontium manganese oxide, $\text{La}_{0.77}\text{Sr}_{0.20}\text{Al}_{0.9}\text{Mn}_{0.1}\text{O}_3$ (LSAM), was joined to stabilized tetragonal zirconia polymorph YTZP (ZrO_2)_{0.97}(Y_2O_3)_{0.03} by a uniaxial stress (3–6 MPa) and high-temperature (1250–1350 °C) bonding method that initiates grain-boundary sliding between the ceramic components. The flow stress of LSAM was larger than that of $\text{La}_{0.8}\text{Sr}_{0.2}\text{Mn}_{0.3}$ under the same test conditions. Electron microscopy confirmed that intergranular penetration occurred at the joining plane, leading to effective bonding between the two dissimilar ceramics. Raman spectral maps of the joining planes obtained with 2-D Raman microscopy demonstrated the absence of any new phases at the interface.

© 2008 Elsevier B.V. All rights reserved.

Keywords: Lanthanum strontium aluminum manganese oxide; LSAM; LSM; Ceramic conductor; Fuel cell; Sensor; Raman microscopy

1. Introduction

Ytria-stabilized zirconia (YSZ) is a solid electrolyte used in high-temperature devices such as fuel cells and oxygen sensors that exploit its high ionic conductivity [1]. Lanthanum strontium manganese oxide, $\text{La}_x\text{Sr}_{1-x}\text{MnO}_3$ (LSM), is an electroceramic commonly used in tandem with YSZ as a cathode in fuel cells [2]. Aluminum-doped LSM, $\text{La}_x\text{Sr}_{1-x}\text{Al}_y\text{Mn}_{1-y}\text{O}_3$ (LSAM) has been proposed as a replacement for LSM as it has been demonstrated that the Al-doping reduces the creation of interlayers formed via reaction of LSM with YTZP [3]. The predominant product of the reaction reported between LSM and YSZ is an insulating pyrochlore, $\text{La}_2\text{Zr}_2\text{O}_7$ (LZ) [4,5].

For dissimilar materials to be used together in a part or component, they must be joined in a way that can withstand the thermal stresses to which the part will be subjected. One possible method of mating dissimilar materials that meets this requirement is joining by plastic deformation. In this process, two or more materials are bonded together by stressing each material to the point where it deforms plastically and intersperses with the other material. YTZP [6] and LSM [7,8] are both known to deform plastically in the same temperature and stress regime through a grain-boundary-sliding (GBS) mechanism. GBS is a diffusion-controlled process and is generally achieved at approximately one half the melting temperature of the material [9]. It is critical to point out that this joining process is fundamentally different from direct diffusional bonding. Samples joined by direct diffusional bonding do not deform plastically, requiring very smooth surfaces and very high temperatures ($0.8T_m$). Typically, joints created via a plastic flow process are between identical or compositionally graded materials. An example of the use of this joining process between several YTZP pieces has been recently demonstrated in the

* Corresponding authors. Dutta is to be contacted at the Department of Chemistry, The Ohio State University, 100 West 18th Avenue, Columbus, Ohio 43210, United States. Singh, Argonne National Laboratory, 9700 South Cass Avenue, Argonne, IL 60439, United States.

E-mail addresses: dsingh@anl.gov (D. Singh), dutta.1@osu.edu (P.K. Dutta).

sealing of a high-temperature internal-reference oxygen sensor [10].

In the present work, a highly Al-doped polymorph of LSAM is joined to YTZP by plastic flow without any special preparation of the mating surfaces. The microstructure of the interface is examined by electron microscopy. Raman spectroscopic maps of the joining planes are employed to look for chemical reactions between the starting materials and the possible creation of new phases at the interlayers. In this manner, a method of bonding wholly dissimilar components for use in high-temperature environments is enabled. While this highly aluminum-doped perovskite may be unsuitable as an electron carrier [3], successful joining of LSAM to YTZP sets the stage for using more conducting forms of LSAM as an alternative to conventional electrodes in high-temperature applications.

2. Experimental

2.1. Synthesis of LSAM

LSAM powder was synthesized via the solid-state method. Nitrates of La, Sr, and Al (Alfa Aesar) were mixed with the chloride of Mn (Alfa Aesar) in the stoichiometric ratio of La: Sr: Al: Mn, 0.8:0.2:0.9:0.1. The powder mixture was milled (SPEX 5100) at high speed for 5 min and transferred to a covered platinum crucible. The powder mixture was reacted at 1000 °C in air for 4 h and ground in an agate mortar and pestle upon cooling. Following grinding, the powders were calcined at 1200 °C for 50 h to ensure complete reaction. Thereafter, the powder was pressed at 3000 kg into 1.1 cm² pellets and fired in a covered platinum crucible at 1500 °C for 50 h to densify the powders into a pellet suitable for joining. Densified pellets were briefly ground to planarize the mating surfaces.

As-synthesized powders were sent to Galbraith Laboratories, Inc. (Knoxville, TN) for elemental analysis of La, Sr, Al, and Mn content. Powders were dissolved in a molten flux via the lithium metaborate fusion process [11]. The resultant material was digested in acid and the weight percent of La, Sr, Al, and Mn determined by ICP-OES.

2.2. Joining of LSAM to YTZP

Each sample was constructed from the following materials and placed into a high-temperature furnace attached to an Instron Universal Testing Machine (Instron, Model 1125) as shown in Fig. 1. The YTZP wafers were cut from preformed and densified rods/tubes of 3 mol% yttria-stabilized tetragonal zirconia polycrystals (YTZP, average particle size ~0.4 μm) that were purchased from Custom Technical Ceramics, Inc (Arvada, CO). The 8 mol% cubic yttria-stabilized zirconia spacers (YSZ, average particle size ~8 μm) were cut from a rod that was also purchased from Custom Technical Ceramics, Inc.

A pellet of LSAM was deformed at a strain rate ($\dot{\epsilon}$) of $4.5 \times 10^{-5} \text{ s}^{-1}$ to determine the yield stress of the perovskite at 1250 °C. After the yield stress of the LSAM was determined, YTZP/LSAM sandwiches were compressed in a static argon atmosphere at either 1250 or 1350 °C at crosshead speeds

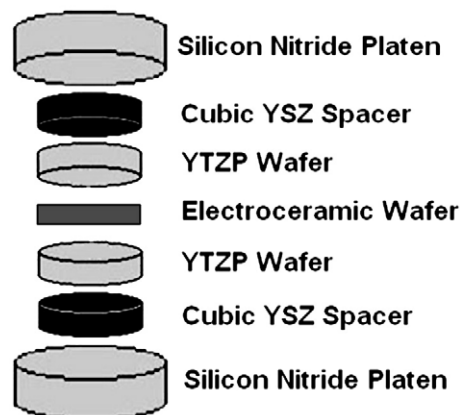


Fig. 1. YTZP/La_{0.77}Sr_{0.20}Al_{0.9}Mn_{0.1}O₃/YTZP joint fabrication scheme. Cubic YSZ spacers and Si₃N₄ platens were removed following joining.

ranging from 0.01 mm/min to 0.02 mm/min resulting in strain rates of $4.5 \times 10^{-5} \text{ s}^{-1}$. During the heating cycle, the load on the sample was controlled as not to exceed 5 N. Upon reaching the target temperature, the system was left under a 5 N load for 30 min to attain thermal equilibrium.

2.3. Characterization techniques

2.3.1. X-ray techniques

The X-ray powder patterns were determined with a Bruker D-8 X-ray diffractometer using nickel-filtered Cu K α ($\lambda = 1.5405 \text{ \AA}$) radiation. Refinements of powder diffraction patterns to extract lattice parameters were performed using the Pawley method [13] as implemented in the TOPAS software package [14]. The quality of the fit is reported as an R_{wp} ; defined as the percent numerical agreement between the calculated and observed intensity profiles, weighted to account for the peak shape variation of experimental data with a finite step size [15]. A low value for R_{wp} indicates a good fit. An R_{wp} of 0 indicates that a pattern has been perfectly fit.

2.3.2. Microscopy

SEM micrographs were obtained using a Philips XL-30 Sirion ESEM. In order to view the joints, sandwiches were cross-sectioned and polished. Following polishing, the samples were mounted onto aluminum pegs with double-sided carbon tape and coated with evaporated gold.

2-D Raman microscopy maps of the YTZP/LSAM interface and data analysis were performed on a Renishaw InVia Raman Microscope. The microscope was operated in line focus mode with 514 nm illumination. Each data point in the map was illuminated for 20 s and collection at each point was repeated two times during map creation. The step size in the x - (perpendicular to joining plane) and y -directions (parallel to joining plane) was 0.5 and 1.056 μm, respectively. The dimension of the line-focused laser beam was 1 by 32.14 μm. The 1 μm beam width and 0.5 μm step in the x -axis allowed distinct regions of the $> 1000 \mu\text{m}^2$ scan area to be identified during collection.

Following collection, the spectrum generated at each point was subjected to Principal Component Analysis (PCA) and then

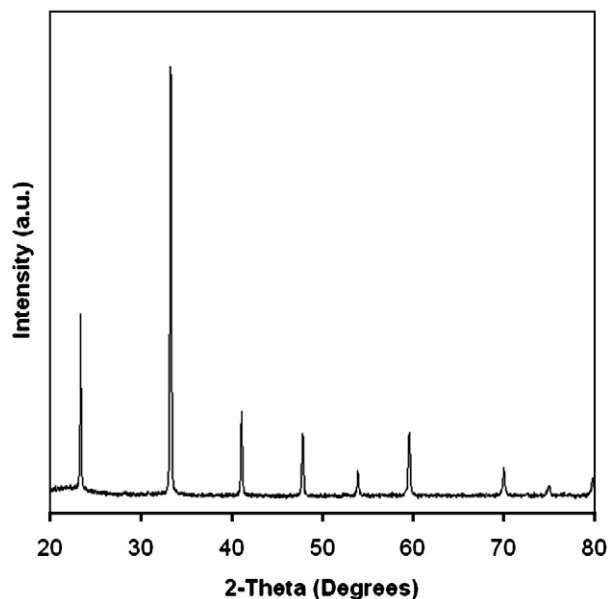


Fig. 2. XRD pattern of $\text{La}_{0.77}\text{Sr}_{0.20}\text{Al}_{0.9}\text{Mn}_{0.1}\text{O}_3$ densified at 1500 °C.

compared to a series of standards. These standards were wafers of LSAM and YTZP that had not undergone the joining process. Comparison of the standard to the collected spectra made it possible to assign each spectrum a score that indicated how similar it was to a standard. The spectrum of a perfect match was designated as $\geq 90\%$ similar to the spectrum of the standard. A successful match to a standard was assigned a color. Within the window of 0 to 90% similarity this color is dimmed or brightened based on proximity to either extreme — the latter being the brightest. In this manner it was possible to map the components in a given region and gauge their reactivity with a neighboring phase.

In all cases the mapping process generated thousands of spectra. Each spectrum was analyzed to check for changes in peak position. For the majority of spectra, changes in absolute peak intensity were common, but changes in relative intensity between neighboring peaks were comparable. The following changes in the observed spectra were used to indicate distinct regions; peak shifts of more than 5 cm^{-1} , a change in relative intensity, or the appearance of a new peak. Representative spectra are presented from each distinct region where these conditions were met.

3. Results

3.1. Synthesis and characterization of LSAM

LSAM was synthesized via the solid-state method from the nitrates of La^{3+} , Sr^{2+} , Al^{3+} and the chloride of Mn^{2+} by heating for 4 h at 1000 °C, grinding the product, then heating the ground mixture for 50 h at 1200 °C. The weight percentages of La, Sr, Al, and Mn determined by ICP-OES were 54.1, 7.98, 2.48, and 11.48%, respectively. These weight percentages correspond to a polymorph of the formula $\text{La}_{0.77}\text{Sr}_{0.20}\text{Al}_{0.9}\text{Mn}_{0.1}\text{O}_3$. The molecular weight of this compound is 202.067 g/mol. A two-

point resistivity measurement [8] was performed of the densified wafer at 1000 °C and yielded a resistivity of $0.15\ \Omega\ \text{cm}$. Holc et al. [3] reported a resistivity for a 94% Al-doped polymorph of LSAM as $\sim 300\ \Omega\ \text{cm}$ at 1000 °C. The improved conductivity of the sample presented in this work is attributed to better densification as the 94% Al-doped polymorph reported previously sintered poorly [3].

The powder diffraction pattern of $\text{La}_{0.77}\text{Sr}_{0.20}\text{Al}_{0.9}\text{Mn}_{0.1}\text{O}_3$ is presented in Fig. 2. No impurities or secondary phases were detected. The six peaks between 20 and 80° 2θ observed were 23.36°, 33.28°, 41.12°, 47.83°, 53.93°, 59.57°, 70.03°, 75.09°, and 79.89°. The peak positions and intensities indicate that the solid-state synthesis produced a material adopting a perovskite structure. This was expected based on the results of previous work which noted that partial substitution of Al for Mn with the general $\text{La}_{0.8}\text{Sr}_{0.2}\text{Al}_x\text{Mn}_{1-x}\text{O}_3$ formula will produce a single phase perovskite material [3,16]. The ternary phase diagram presented by Kuscer et al. [17] in the $\text{LaMnO}_{3+\delta}$, $\text{SrMnO}_{3-\delta}$, LaAlO_3 system indicates the possible presence of SrAl_2O_4 , $\text{LaMn}_{1-x}\text{Al}_x\text{O}_3$, and $\text{La}_{1-y}\text{Sr}_y\text{MnO}_3$. However, no ternary or quaternary oxides other than LSAM are detected in the diffraction pattern.

A Pawley fit was performed on the diffraction pattern in Fig. 2 in order to determine the lattice parameters. Cubic space group $Fm\bar{3}m$ (#225) was selected for the fit as there was no peak splitting to indicate a lower symmetry cell. The calculated lattice parameter of the cubic cell was 3.79627(21) Å with an R_{wp} of 3.3. This estimate of cell volume was used to calculate the theoretical density of densified LSAM as $6.1\ \text{g/cm}^3$. The density of a sintered pellet was measured by Archimedes method as $5.6\ \text{g/cm}^3$, indicating that pellets densified for 50 h at 1500 °C were $\sim 92\%$ dense. Following densification the average particle size of LSAM was estimated by SEM as $\sim 2\ \mu\text{m}$.

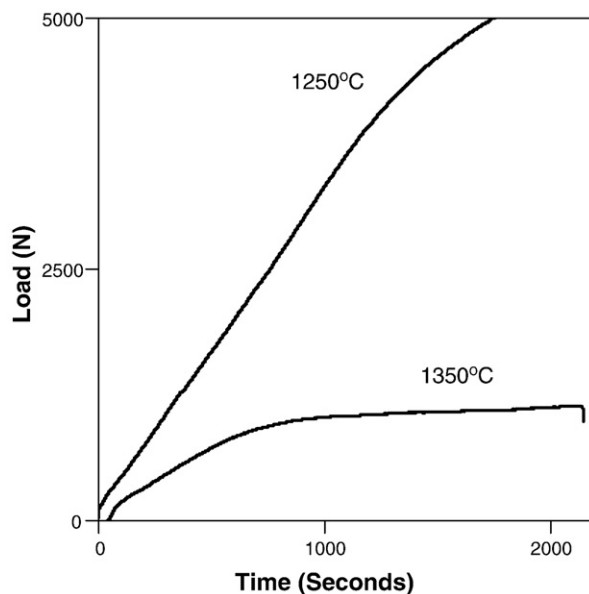


Fig. 3. Load versus time curve for $\text{La}_{0.77}\text{Sr}_{0.20}\text{Al}_{0.9}\text{Mn}_{0.1}\text{O}_3$ sandwiched between wafers of YTZP at 1250 and 1350 °C.

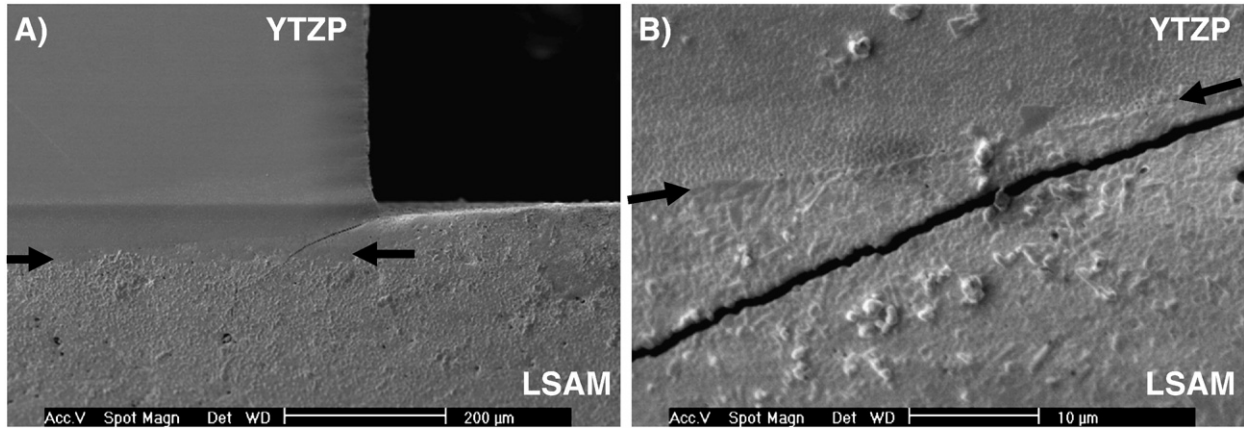


Fig. 4. Joining plane of $\text{La}_{0.77}\text{Sr}_{0.20}\text{Al}_{0.9}\text{Mn}_{0.1}\text{O}_3$ joined to YTZP at 1250 °C. Arrows denote the joining plane. A) Wide view of joint. B) Same joint at higher magnification. (Crack is probably a result of sample sectioning. The crack does not go through the joining plane.)

3.2. Deformation and joining results

Compressive deformation of LSAM at $\dot{\epsilon} = 4.5 \times 10^{-5} \text{ s}^{-1}$ and 1250 °C resulted in a steady-state stress of $\sim 36 \text{ MPa}$. The load versus time curve for the joining of YTZP to LSAM at 1250 and 1350 °C is shown in Fig. 3. The load was applied until the maximum of the load cell (5 kN) was reached or a steady-state was established. At this time, the load was backed off and the amount of plastic deformation recorded. For samples joined at 1250 and 1350 °C, $\Delta L/L \sim 3.5\text{--}7\%$ were observed. L is the height of the YTZP/LSAM/YTZP sandwich prior to joining. At 1350 °C the stress on the sandwich was $\sim 10 \text{ MPa}$.

3.3. Microstructure of joining planes

SEM micrographs of the joints produced at 1250 and 1350 °C at two different magnifications are presented in Figs. 4 and 5, respectively. As there are two distinct materials, the joining planes are clearly distinguishable from the bulk ceramics (indicated by arrows in each image). The porosity of LSAM observed in Figs. 4 and 5 is the result of imperfect

densification. A high-resolution SEM image of the joint produced at 1250 °C is presented in Fig. 6.

LSAM wafers were not perfectly cylindrical and slightly larger than YTZP wafer. In locations where the width of the LSAM wafer exceeded that of the YTZP wafer, as exhibited in Fig. 4A, the YTZP penetrated LSAM such that the true joining plane is several microns below the point of contact prior to joining. Cracking is observed in Fig. 4A and B and above the joining plane in Fig. 5A. As all cracks tend to be away from the joining plane, it is believed they are artifacts of the cutting process.

3.4. Raman microscopy

Spectra were taken of unjoined YTZP and LSAM wafers of as controls. The spectrum of YTZP in Fig. 7C exhibited peaks at 146, 260, 322, 402, 463, 642, 957, and 1001 cm^{-1} , consistent with literature [18]. The spectrum of unjoined LSAM in Fig. 7A exhibited peaks at 567 and 745 cm^{-1} . As shown in Figs. 4 and 5, LSAM exhibited signs of porosity. The spectrum in Fig. 7B was collected from a porous region of the LSAM control. As

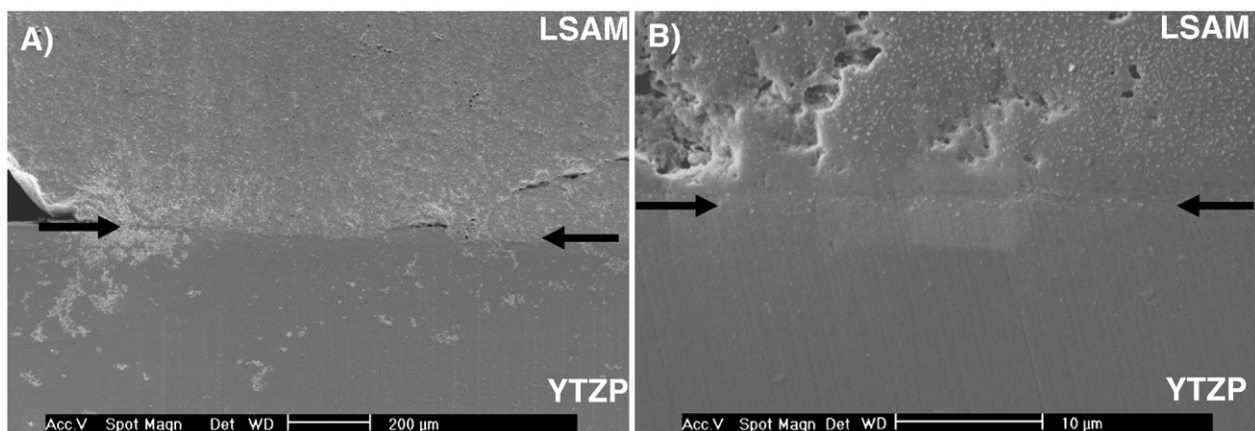


Fig. 5. Joining plane of $\text{La}_{0.77}\text{Sr}_{0.20}\text{Al}_{0.9}\text{Mn}_{0.1}\text{O}_3$ joined to YTZP at 1350 °C. Arrows denote the joining plane. A) Wide view of joint. B) The same joint viewed at higher magnification exhibits that a joint was created even though the material is not fully dense. There is a rectangle of light contrast in the middle of the image due to charging from a previous image taken at high resolution.

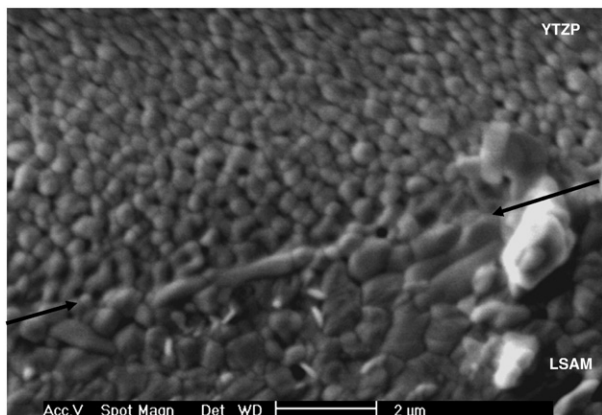


Fig. 6. High-resolution SEM of the joining plane in YTZP/LSAM/YTZP joined at 1250 °C.

compared to Fig. 7A, there is a shift of the 567 cm^{-1} peak to 570 cm^{-1} , along with a significant increase in intensity. The intensity variation is attributed to the crystallites within pores under less strain than crystallites located in fully dense regions [19].

Raman maps along the joining plane between YTZP and LSAM are presented in Figs. 8 and 9. The scanned regions are presented within the view from the 50× objective so the joining plane is clearly visible. In this manner, it is possible to determine the extent to which the LSAM phase reacted with the YTZP. The laser was line-focused to a $1 \times 32\text{ }\mu\text{m}^2$ illumination area and moved across the joining plane in $0.5\text{ }\mu\text{m}$ increments in the x -direction and $1.056\text{ }\mu\text{m}$ increments in the y -direction. In the samples joined at 1250 and 1350 °C, the sizes of the scanned areas were $67 \times 32\text{ }\mu\text{m}$ and $37 \times 62\text{ }\mu\text{m}$, respectively. The large

area marked in green in Figs. 8 and 9 is a $\geq 90\%$ match to the YTZP control (Fig. 7C). The representative spectrum of the green region is shown in Figs. 8A and 9A. The large region on the right marked in red is a $\geq 90\%$ match to the LSAM control (Fig. 7B). The representative spectrum of the red region is shown in Figs. 8C and 9C. Within the bulk of the red region, islands of poor comparisons are noted by dark spots due to mismatch with the control LSAM sample. These regions exhibit an intensity change of the spectral feature found at 567 cm^{-1} as shown in the difference between spectra 7a and 7b. This change in intensity accounts for the poor scoring.

The joining plane is the narrow region sandwiched between the green-labeled YTZP bulk and red-labeled LSAM bulk. This region is marked as JP and designated as the thin black area between the arrows in Figs. 8 and 9. Raman spectra from the joining plane exhibit features of YTZP and LSAM. The representative spectra from this region are shown in Figs. 8B and 9B. No new Raman peaks indicate the absence of any new phases in the joining plane.

4. Discussion

4.1. Joining and microstructure

Pure LSM, when deformed in static argon at 1250 °C, exhibits a near-zero yield stress [7]. Therefore, it was necessary to determine if the strain rates required to deform YTZP, $\sim 40\text{ MPa}$ at 1250 °C, would overstress the LSAM during joining [12].

As the steady-state stress of LSAM at $\dot{\epsilon} = 4.5 \times 10^{-5}\text{ s}^{-1}$ and 1250 °C is $\sim 36\text{ MPa}$, it is similar to that of YTZP and therefore a good candidate for joining. This steady-state stress is at least a factor of ten higher than the steady-state stress of LSM [7],

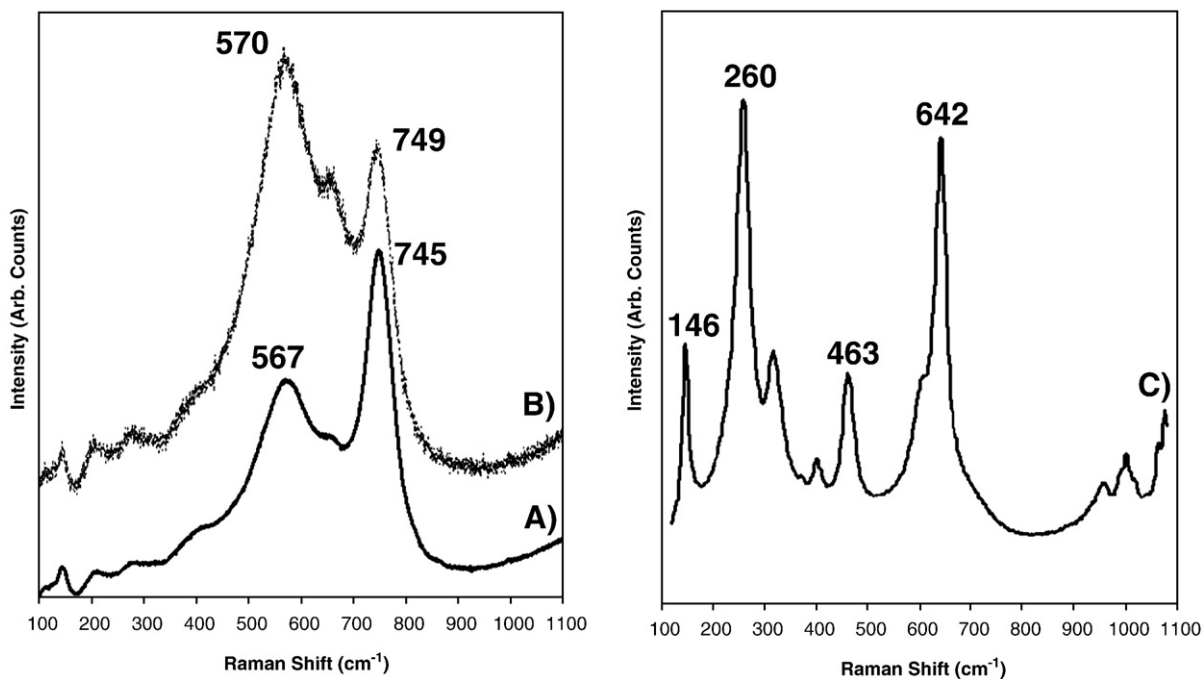


Fig. 7. A) Raman spectrum of an unjoined $\text{La}_{0.77}\text{Sr}_{0.20}\text{Al}_{0.9}\text{Mn}_{0.1}\text{O}_3$ pellet densified at 1500 °C. B) Raman spectrum of a pore within the densified mass of $\text{La}_{0.77}\text{Sr}_{0.20}\text{Al}_{0.9}\text{Mn}_{0.1}\text{O}_3$. C) Raman spectrum of an unjoined wafer of YTZP.

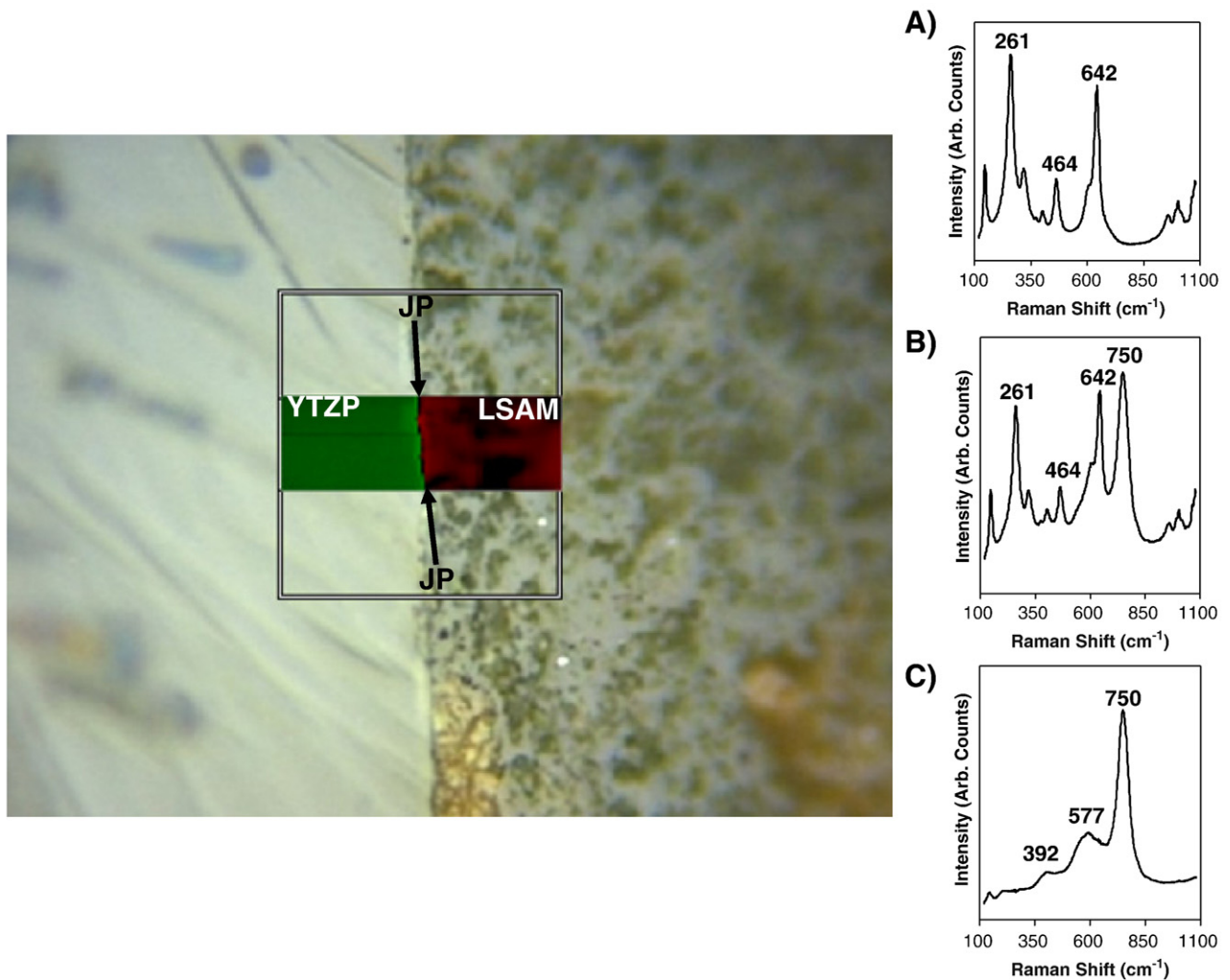


Fig. 8. Raman map of YTZP/La_{0.77}Sr_{0.20}Al_{0.9}Mn_{0.1}O₃/YTZP interface in sample joined at 1250 °C. The joining plane is the narrow region denoted as JP that lies between the bulk of YTZP and LSAM. A) Representative spectrum of the YTZP region marked in green. B) Representative spectrum of the joining plane denoted by arrows. C) Representative spectrum of the LSAM region marked in red. (For interpretation of the references to color in this figure legend, the reader is referred to the web version of this article.)

implying that substitution of aluminum for manganese on the B-site of the perovskite hardens LSM. Since the deformation of LSAM was performed at one temperature and strain rate, it would be speculative to assign a physical mechanism to this increased flow stress.

As expected, the stress required to join LSAM to YTZP at the temperature of 1350 °C was reduced compared to that at 1250 °C. This is clearly evident in the lower slope of the load versus time curve in Fig. 3. The plasticity of YTZP in the sub-micron particle size range is known to increase with temperature as GBS is a diffusion-controlled process [6]. This increase in plasticity of the YTZP will contribute in lowering the steady-state stress at a given strain rate. Given the relatively low temperatures ($<0.8T_m$ usually required for deformation bonding) used for joining and the clear grain intermingling at the joining plane, there is strong evidence that YTZP and LSAM are plastic in the same stress regime. However, a more detailed study of the steady-state creep at several different temperatures

would be required to determine the activation energy for grain-boundary sliding in LSAM to prove this hypothesis.

Another possible contributor to the enhanced accommodation of the applied load at 1350 °C is densification of the LSAM that could take place simultaneously during the joining process. The SEM images in Figs. 5 and 6 indicate that LSAM is not fully dense. Holc et al. [3] report poor LSAM pellet densification in a 94% Al-doped polymorph, noting the resultant powder barely sintered. Even though pelletization was possible at 1500 °C, there was residual porosity. Future joining experiments may require a higher pelletization temperature for LSAM to ensure that the densest possible material is used for creating a joint. Irrespective of these factors contributing to accommodating the load during joining, the intermingling of grains over the entire joining plane is clearly visible in Figs. 4–6, even at 1250 °C, indicating that plastic flow may have occurred via GBS, as shown for many fine-grained ceramics [6–9].

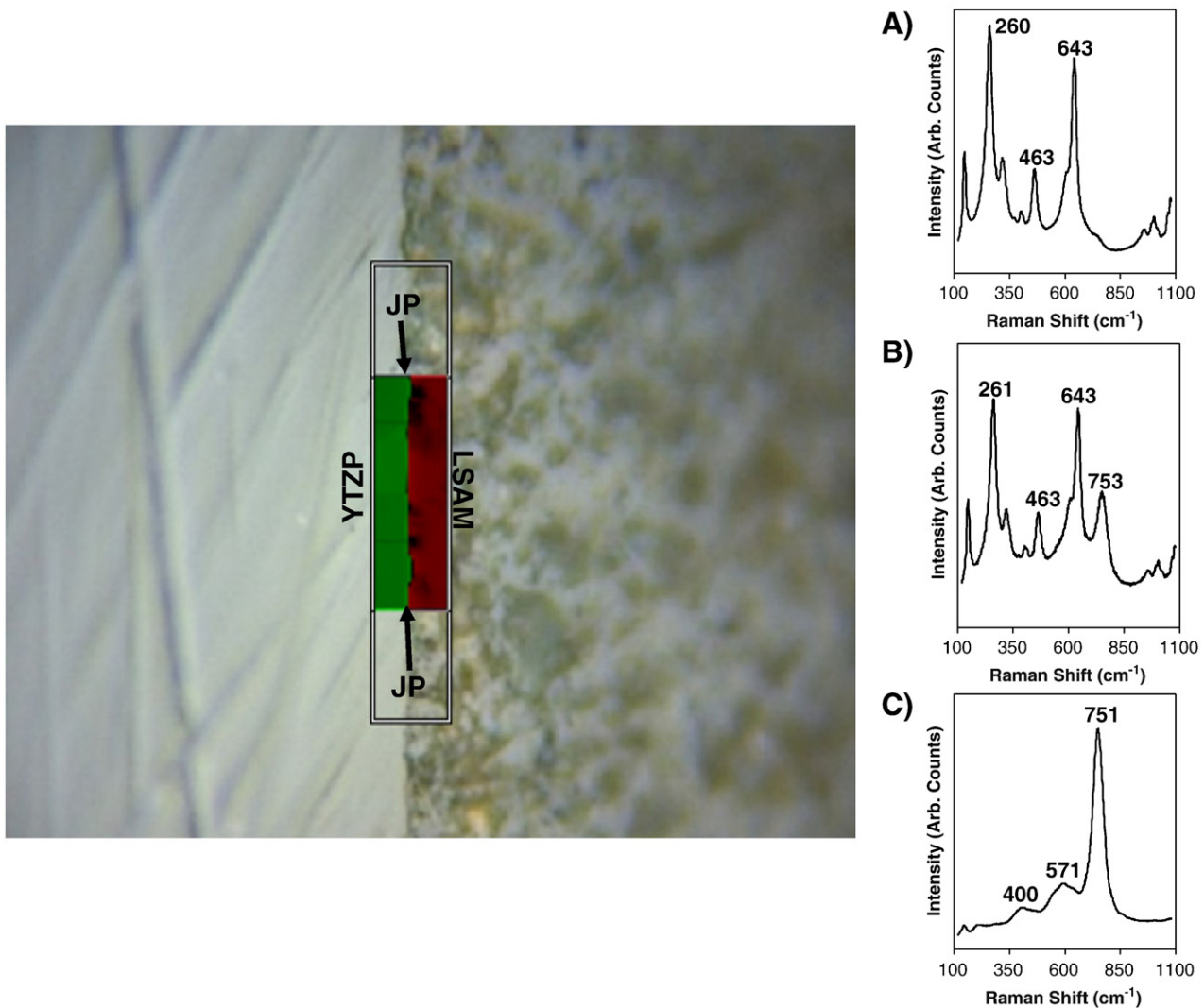


Fig. 9. Raman map of YTZP/La_{0.77}Sr_{0.20}Al_{0.9}Mn_{0.1}O₃/YTZP interface in sample joined at 1350 °C. The joining plane is the narrow region denoted as JP that lies between the bulk of YTZP and LSAM. A) Representative spectrum of the YTZP region marked in green. B) Representative spectrum of the joining plane denoted by arrows. C) Representative spectrum of the LSAM region marked in red. (For interpretation of the references to color in this figure legend, the reader is referred to the web version of this article.)

4.2. Raman microscopy of joining planes

In samples joined at both 1250 and 1350 °C, Raman peaks from the YTZP bulk match that of unjoined YTZP and are represented by the bright green coloration at the left side of the scanned areas in Figs. 8 and 9. Raman peaks from the LSAM bulk that match that of unjoined LSAM are highlighted in red on the right side of the scanned area in Figs. 8 and 9. However, there are regions of poor scoring in the LSAM bulk (darker spots amidst the LSAM bulk in Figs. 8 and 9) induced by a change in intensity of the 567 cm⁻¹ band. As shown by the difference in Fig. 7A and B, the change in intensity of this band is attributed to a lower strain upon the crystallites within pores as opposed to the densified crystallites of the bulk. Strain inhomogeneity within a sample has been analyzed in the past with Raman microscopy for SiC and an intensity increase is noted in regions of comparatively lower strain [19]. It is important to note that regions of poor scoring were diminished for

the sample joined at 1350 °C as the higher temperature likely eliminated some of the porosity present before joining. Other than this change in relative intensity, samples joined at both 1250 and 1350 °C exhibited no new peaks in the bulk of either YTZP or LSAM.

The joining planes marked as B in Figs. 8 and 9 track the transition between phases and exhibit a combination of the Raman bands for LSAM and YTZP. As the laser focus is 1 μm in width and moved along the joining plane in 0.5 μm increments it is possible to identify new compounds at the interface by changes in spectral features. Based on the sharp Raman spectral transition between phases in Figs. 8 and 9, and the absence of any new Raman bands, we conclude no La₂Zr₂O₇ [20] (LZ) or other phases are present in the joining plane. The lack of LZ in a joining plane is important in the creation of durable joints as LZ exhibits a significantly different thermal expansion coefficient (TEC) than that of stabilized zirconia [21,22].

4.3. Conclusion

$\text{La}_{0.77}\text{Sr}_{0.20}\text{Al}_{0.9}\text{Mn}_{0.1}\text{O}_3$ exhibits plasticity in the same temperature and stress regime as YTZP, allowing for the creation of pore-free joints via a lower-temperature alternative to diffusion bonding. Electron microscopy of the joining planes indicate that even though residual porosity of the LSAM persists through the joining process, the grains at the mating points of each surface have intermingled, likely as a result of simultaneous grain-boundary sliding. The high aluminum content of LSAM inhibits reaction with YTZP and therefore the production of interlayers which would serve to diminish the quality of the joint. This is confirmed by the absence of new bands in the Raman spectral maps of the bulk material and joining planes. By choosing a composition of LSAM that does not react with YTZP, it is possible to create joints between these two dissimilar materials without an intermediate bonding agent or compositionally graded interlayer.

Acknowledgements

The work was supported by the Office of FreedomCAR and Vehicle Technologies of the U.S. Department of Energy, at Argonne National Laboratory managed by UChicago, Argonne, LLC under contract No. DE-AC02-06CH11357. The work at The Ohio State University was supported by the Department of Energy (DE-FC26-03NT41615).

References

- [1] R. Ramamoorthy, D. Sundararaman, S. Ramasamy, *Solid State Ionics* 123 (1–4) (1999) 271.
- [2] T. Suzuki, M. Awano, P. Jasinski, V. Petrovsky, H.U. Anderson, *Solid State Ionics* 177 (2006) 2071.
- [3] J. Holc, D. Kuščer, M. Hrovat, S. Bernik, D. Kolar, *Solid State Ionics* 95 (1997) 259.
- [4] S.P. Jiang, J-P. Zhang, K. Föger, *J. Eur. Ceram. Soc.* 23 (2003) 1865.
- [5] A. Mitterdorfer, L.J. Gauckler, *Solid State Ionics* 111 (1998) 185.
- [6] M. Jimenez-Melendo, A. Dominguez-Rodriguez, A. Bravo-León, *J. Am. Ceram. Soc.* 81 (1998) 2761.
- [7] R.E. Cook, K.C. Goretta, J. Wolfenstine, P. Nash, J.L. Routbort, *Acta Mater.* 10 (1999) 2969.
- [8] F. Gutierrez-Mora, J.L. Routbort, *J. Am. Ceram. Soc.* 85 (2002) 2370.
- [9] R. Raj, M.F. Ashby, *Metall. Trans.* 2 (1971) 1113.
- [10] J.V. Spirig, R. Ramamoorthy, S.A. Akbar, J.L. Routbort, D. Singh, P.K. Dutta, *Sens. Actuators, B, Chem.* 124 (2007) 192.
- [11] S.V. Panteeva, D.P. Gladkochoub, T.V. Donskaya, V.V. Markova, G.P. Sandimirova, *Spectrochim. Acta, Part B: Atom. Spectrosc.* 58B (2003) 341.
- [12] J.L. Routbort, *Acta Met.* 27 (1979) 649.
- [13] G.S. Pawley, *J. Appl. Crystallogr.* 14 (1981) 357.
- [14] R.W. Cheary, A. Coelho, *J. Appl. Crystallogr.* 25 (1992) 109.
- [15] R.J. Hill, R.X. Fischer, *J. Appl. Crystallogr.* 23 (1990) 462.
- [16] Q.X. Fu, F. Tietz, P. Lersch, D. Stöver, *Solid State Ionics* 177 (2006) 1819.
- [17] D. Kuščer, M. Hrovat, J. Holc, S. Bernik, D. Kolar, *Mater. Res. Bull.* 35 (2000) 2522.
- [18] P. Duran, F. Capel, C. Moure, A.R. Gonzalez-Elipse, A. Caballero, M.A. Banares, *J. Electrochem. Soc.* 146 (1999) 2425.
- [19] L.A. Falkovsky, J.M. Bluet, J. Camassel, *Phys. Rev., B* 55 (1997) R14697.
- [20] D. Michel, M. Perez y Jorba, R. Collongues, *Mater. Res. Bull.* 9 (1974) 1457.
- [21] K. Bobzin, E. Lugscheider, N. Baccivan, *Adv. Eng. Mater.* 8 (2006) 653.
- [22] F.M. Figueiredo, F.M.B. Marques, J.R. Frade, *J. Electroceram.* 7 (2001) 47.